Citation
Chen, W. and Shaikh, F. and Li, Z. and Ran, W. and Hao, H. 2021. Dynamic compressive properties of high volume fly ash (HVFA) concrete with nano silica. Construction and Building Materials. 301: ARTN 124352. http://doi.org/10.1016/j.conbuildmat.2021.124352

Dynamic compressive properties of high volume fly ash (HVFA) concrete with nano silica

Wensu Chen*, Faiz Shaikh, Zhixing Li, Wenlong Ran and Hong Hao*

Center for Infrastructural Monitoring and Protection, School of Civil and Mechanical Engineering, Curtin University, Australia

**Corresponding authors: wensu.chen@curtin.edu.au (W. Chen); hong.hao@curtin.edu.au (H. Hao)*

Abstract

High Volume Fly Ash (HVFA) concrete enables the utilization of fly ash (FA) to diminish greenhouse gas emission by decreasing the demand of ordinary Portland cement. Structures made of HVFA concrete, such as roadside barriers, tunnel cushions and building walls could be subjected to impact and blast loads during service life. Thus, dynamic performance of HVFA concrete is worthy of investigating for better analysis and design of concrete structures. This paper presents the quasi-static and dynamic properties of HVFA concrete containing FA contents of 40 and 60% (by wt.) as partial replacement of cement. The effect of 2% (by wt.) nano silica (NS) on the quasi-static and dynamic properties of HVFA concrete is also studied. The dynamic compressive tests are carried out by using a split Hopkinson pressure bar (SHPB) with 100 mm diameter. The failure processes and patterns as well as stress-strain curves of plain and HVFA concretes under different strain rates are compared. The strain rate effects on the compressive strength, modulus of elasticity and energy absorption capacities are analysed. The experimental results show that quasi-static and dynamic performances of HVFA concrete are enhanced by the addition of NS. With the increase of FA content, the damage level becomes more severe, and modulus of elasticity and energy absorption capacities of HVFA concretes become lower at the similar strain rate. Dynamic increase factors (DIF) of compressive strength for HVFA concretes are quantified and compared with the empirical formulae recommended by Euro-International Committee for Concrete (CEB) for normal concrete. Adding NS leads to lower DIF for compressive strength of HVFA concrete. Empirical formulae for DIF of compressive strength, modulus of elasticity and energy absorption capacity of HVFA concretes with and without nano silica as a function of strain rate are proposed. It is worth noting that the NS modified HVFA C60F38N2 in this study has higher compressive strength, modulus of elasticity and energy absorption capacity than the plain concrete (PC), which shows the potential to replace the normal concrete as a sustainable construction material.

Keywords: High Volume Fly Ash (HVFA) concrete; Nano silica; SHPB; Dynamic compressive properties; Impact loading; Energy absorption.

1. Introduction

Conventional concrete has been used intensively as construction material around the world. Ordinary Portland cement (OPC) is the main constituent of concrete. The annual consumption of OPC is around 4.3 billion tons and the global production grows by 9% annually in recent years [1-3]. The increasing demand of OPC has attracted the concern of environmental issues because a ton of carbon dioxide is released from manufacturing one ton of OPC. It is reported that the emissions of greenhouse gas from producing OPC account for 6% of global emissions [4]. In this regard, industrial waste or by-products, such as fly ash (FA), rice husk ash and slag can be used to diminish environmental impact by partially replacing OPC. High volume fly ash (HVFA) concrete by replacing at least 40% OPC with FA can improve the sustainability and workability of concrete [5-9]. However, there are several drawbacks of replacing OPC with FA, i.e. inferior mechanical properties at an early age because of the slow pozzolanic reaction of FA. To overcome the shortcoming, nanomaterials with smaller particle size and larger surface area than FA can be used as cementitious additives in the HVFA concrete. The mechanical properties of HVFA concrete at an early age can be improved by virtue of early hydration reaction between nanomaterial and calcium hydroxide as well as the filling effect of nanoparticles in the micro-voids.

Nanomaterials, such as nano silica (NS), refer to the materials with the nanoscale size or bulk materials containing nano-sized particles with the diameter less than 100 nm. NS is classified as an advanced pozzolan, which improves mechanical behaviors and modifies the microstructural cement-based material [10]. When NS is added to the cement-based system, the filling effect leads to the immobilization of free water. The micro-voids in the matrix are filled by NS particles to form the dense microstructure. Besides, the bond strength of interfacial transition zone (ITZ) between aggregates and matrix is enhanced by incorporating nanoparticles due to the formation of calcium–silicate–hydrates (C–S–H) gel during pozzolanic reactions [11]. Thus, the early age strength and the durability of concrete containing high volume FA can be significantly improved by adding NS particles.

The effects of NS addition on quasi-static properties of HVFA concrete have been investigated in the previous studies. It was reported that the compressive strength of HVFA concrete containing 50% FA was enhanced by substituting FA with 4% [12] and 1% [13] (by wt.) of NS content. Shaikh et al. [9] reported that the addition of 2% NS as FA replacement in HVFA concretes containing 40 to 70% FA obtained the highest compressive strength at 7 days and 28 days. Shaikh and Supit [11] revealed that the addition of 2% NS improved the performance of HVFA concrete due to the modified microstructure.

Engineering structures might be subjected to dynamic loads such as blast and impact loads during their service life. Thus, dynamic properties of concrete material are essential for the accurate predication of structural performance under various strain rates. However, the studies on the dynamic behaviours of HVFA concrete and nano silica modified HVFA concrete under high strain rates are very limited. Zhou et al. [14] investigated dynamic properties of HVFA mortar without nano silica at different curing ages. Mussa et al. [15] compared the dynamic behaviours of HVFA concretes containing 52.5% of FA and 2.5% NS (by wt.) at strain rate ranging from 30.12 to 101.42 s^{-1}. It was reported that the compressive strength, toughness, critical strain and failure mode of HVFA concrete containing NS were sensitive to the strain rate. Mussa et al. [16] further studied dynamic properties of NS modified HVFA concrete with curing age changed from 7 days to 90 days, and reported that the compressive strength of NS modified HVFA concrete with the longer curing age was more sensitive to strain rate, demonstrated by the higher dynamic increase factor (DIF). It should be noted that the previous studies have investigated dynamic properties of NS modified HVFA concrete. However, the comparison of dynamic behaviour between HVFA concrete and NS modified HVFA concrete (i.e. the effect of NS addition on dynamic behaviours) has not been revealed, which is deemed necessary for study.

In a previous study [9], quasi-static compressive properties of HVFA concretes containing 40% and 60% FA with 2% nano silica (by wt.) have been studied. As an extension of the previous study [9], quasi-static test on the HVFA concrete is also conducted, which serves as a reference for dynamic tests. A Ø100-mm split Hopkinson pressure bar (SHPB) system is used to obtain dynamic compressive properties of HVFA concretes with/without nano silica with the strain rate up to 149.49 s^{-1}, including failure mode, dynamic strength, modulus of elasticity and energy absorption capacities of concrete mixes. Dynamic increase factors (DIF) of compressive strength for HVFA concretes are compared with the formulae recommended by Euro-International Committee for Concrete (CEB). The formulae for dynamic increase factor (DIF) of compressive strength, modulus of elasticity and energy absorption capacity of HVFA concrete with/without nano silica are proposed.

2. Experimental program

2.1. Material

As an extension of the previous study [9], the dynamic compressive properties of HVFA concretes with/without NS are investigated in this study. Therefore, the similar raw materials are used to get the consistent mix as the previous study [9]. Type I ordinary Portland cement was supplied by Cockburn Cement, Australia. The commercially available silica sand was sourced from Hanson Construction Materials. Low calcium class F fly ash (FA) was supplied by the Gladstone power station. Nano silica (NS) was obtained from MK Impex Corp, Canada. The chemical compositions and physical properties of ingredients are given in Table 1 and Table 2, respectively.

Table 1. Chemical compositions of cement, fly ash and nano silica [9].

Composition (wt. %)	SiO_2	Al_2O_3	Fe_2O_3	CaO	MgO	MnO	K_2O	Na_2O	P_2O_5	TiO_2	SO_3
Cement	20.2	4.9	2.8	63.9	2.0	-	-	-	-	-	2.40
Fly ash (FA)	51.80	26.40	13.20	1.61	1.17	0.10	0.68	0.31	1.39	1.44	0.21
Nano silica (NS)	99	-	-	-	-	-	-	-	-	-	-

Table 2 Properties of cement, fly ash and nano silica [9].

Compounds	Particle size	Specific gravity	Surface area (m^2/g)	Loss on ignition (%)
Cement	25-40% <=7um	2.7-3.2	-	2.4
Class F fly ash (FA)	40% of 10 um	2.6	-	0.5
Nano silica (NS)	25 nm	2.2-2.6	160	-

2.2. Mix proportions

In this study, the cement was partially replaced with 40% and 60% (by wt.) FA to cast HVFA concretes. NS content of 2% (by wt.) as partial replacement of FA was the optimum amount based on the previous study [9]. The water/binder ratio of 0.4 and the sand/binder ratio of 2.75 were used for all mixes. A constant superplasticizer dosage of 50 mL was used in all mixes to achieve sound workability for casting. The mix proportions of all concrete mixes are given in Table 3.

Table 3. Mix proportions (unit: kg/m^3).

Mix type	Cement	Class F Fly ash (FA)	Nano silica (NS)	Sand	Coarse aggregate	Water
PC (Plain)	400	-	-	684	1184	163
C60F40	240	160	-	684	1184	163
C40F60	160	240	-	684	1184	163
C60F38N2	260	128	8	684	1184	163
C40F58N2	160	232	8	684	1184	163

2.3. Mixing and curing of specimens

In this study, sand and coarse aggregates in saturated surface dry (SSD) condition were prepared as per ASTM [17]. The NS powder was dispersed in water by using an ultrasonic mixer for about 30 minutes, as shown in Fig. 1. 70 L pan mixer was used for preparing all concrete mixes at an ambient temperature of approximate 25°C. Firstly, cement, FA, sand and coarse aggregates were dry mixed for three minutes. Then, NS dispersed in water and superplasticizer were gradually poured into the dry mixture and mixed for another three minutes. The mixes were then cast in three layers into Ø100 × 200 mm cylindrical specimens with vibration to release the entrapped air bubbles. After demoulding, the specimens were placed in water-curing treatment at 25 °C for 28 days. The Ø100 × 200 mm cylindrical specimens and disc specimens with a size of Ø100 × 50 mm were prepared for the quasi-static and dynamic compressive tests, respectively.

Fig. 1. Ultrasonic mixing of nano silica

2.4. Experimental methodology

2.4.1. Quasi-static compressive test

Fig. 2 shows the test setup for quasi-static compressive tests. Quasi-static compressive tests were carried out with a loading rate of 0.33 MPa/min in accordance with ASTM C39-18 [18]. Three sulphur-capped cylindrical specimens were tested for each mix.

Fig. 2. Set-up of quasi-static compressive tests.

2.4.2. Dynamic compressive test

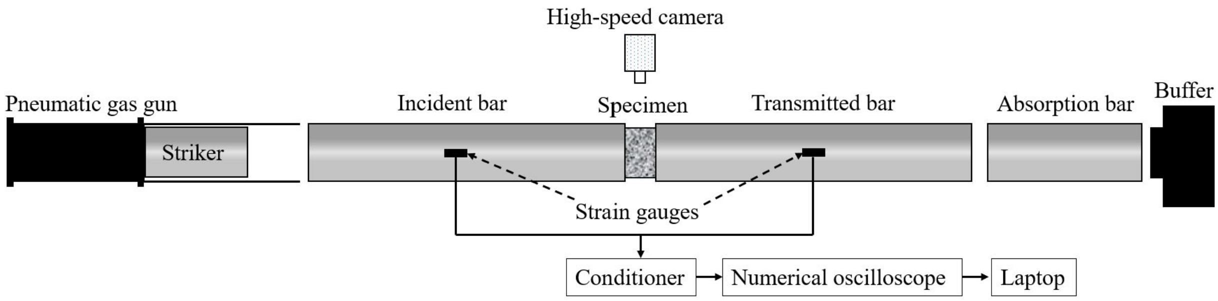

(a)

(b) (c)

Fig. 3. (a) Schematic diagram of set-up; (b) Ø100-mm SHPB system; (c) rubber pulse shaper.

In this study, dynamic compressive tests were carried out by using an Ø100-mm SHPB. The failure process, failure mode, dynamic compressive strength, modulus of elasticity and energy absorption capacities were analysed and compared. At least three specimens were tested under a similar air pressure for each configuration. As shown in Fig. 3 (a), the SHPB test system consists of an incident, transmitted and absorption bar with the length of 5500 mm, 3000 mm and 1000 mm, respectively. A cylindrical striker with the length of 400 mm was used. The strain gauges were attached onto the incident and transmitted bars to record the stress wave signal, respectively. The failure process of the specimens was recorded by using a high-speed camera. In order to minimize the effect of end friction confinement, the grease was applied evenly on the interfaces between the pressure bars and the specimen. Moreover, using pulse shaper can facilitate stress equilibrium by diminishing the high-frequency oscillation and prolonging the rising time of the incident wave [19]. As shown in Fig. 3 (c), a rubber pulse shaper (diameter= 20mm and thickness =3mm) was attached onto the incident bar in this study.

3. Results and discussions

3.1. Quasi-static compressive test

Fig. 4 shows the quasi-static compressive strength of plain and HVFA concrete mixes. As expected, the quasi-static compressive strength decreased with the increase of FA content, i.e. the compressive strength of plain concrete (PC) was 35.18 MPa and the compressive strength decreased by 15% and 40% to 29.64 MPa and 21.13 MPa by replacing 40% and 60% of cement with FA, respectively. Besides, the compressive strength was enhanced by replacing 2% FA with NS. With the replacement of 2% NS, the compressive strength of HVFA concrete containing 38% and 58% FA increased to 37.07 MPa and 23.29 MPa, by 25% and 10%, respectively. It is worth noting that the HVFA concrete containing 38% FA and 2% NS has higher compressive strength than the plain concrete (PC), which indicates the NS modified HVFA concrete material can replace the normal concrete. It should be noted that the effect of the addition of NS on the quasi-static compressive strength of HVFA is consistent with the previous studies [1, 9, 12, 13].

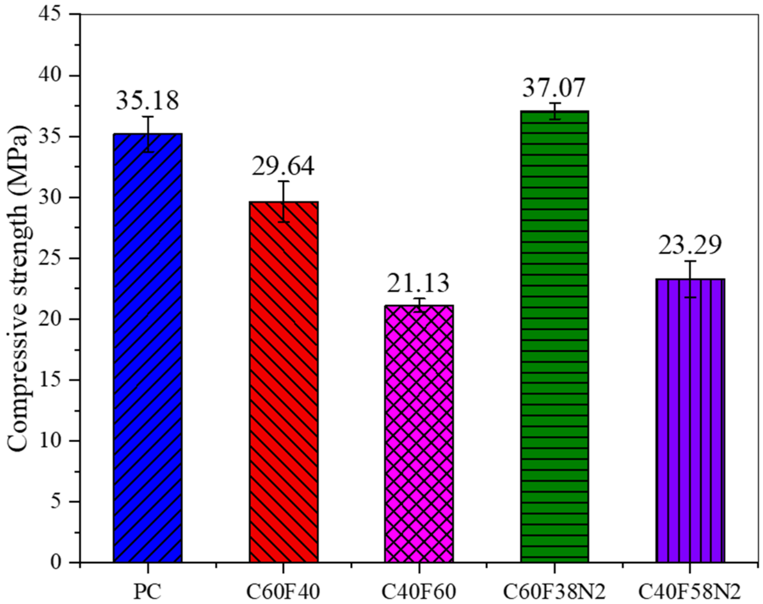

Fig. 4. Quasi-static compressive strength of plain concrete and HVFA concretes w/o NS.

3.2. Validity and strain rate determination of SHPB tests

In this study, the typical half-sine wave signals were obtained by using the rubber pulse shaper as shown in Fig. 5. One-dimensional wave propagation theory is applied in the SHPB technique. The stress (σ), strain rate ($\dot{\varepsilon}$) and strain (ε) of the specimens can be calculated by the equations (1-3) [20], respectively.

$$\sigma(t) = E_b(\frac{A_b}{A_s})\varepsilon_T(t) \quad (1)$$

$$\dot{\varepsilon}(t) = \frac{2C_0}{L}\varepsilon_R(t) \quad (2)$$

$$\varepsilon(t) = \int_0^T \dot{\varepsilon}\,(t)dt \quad (3)$$

where E_b, A_b and C_0 represents the modulus of elasticity, cross-section area and elastic wave velocity of the pressure bars, respectively; A_s and L stand for the cross-section area and length of the specimen, respectively; ε_T and ε_R are the time-dependent transmitted and reflected strain, respectively.

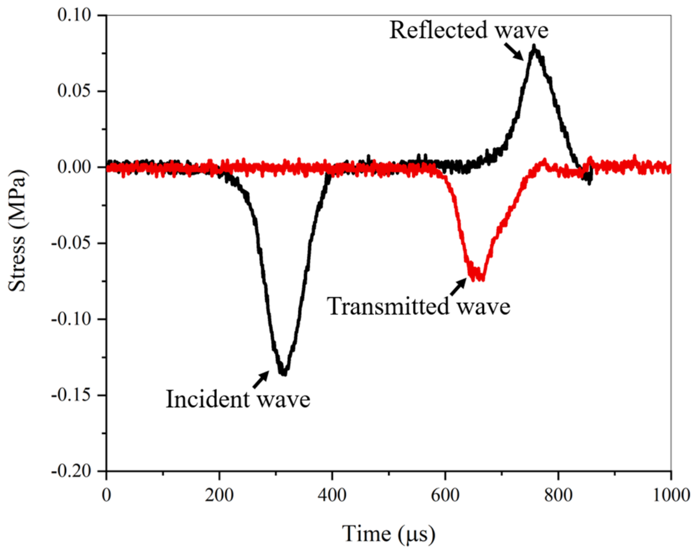

Fig. 5. Typical signal waveform.

It is worth noting that stress equilibrium has to be satisfied to ensure the validity of test data for the SHPB tests. Stress equilibrium indicates that the ‘‘incident + reflected” stress wave is in good match with the transmitted stress wave. The stress equilibrium conditions of representative plain and HVFA concrete specimens were reached as shown in

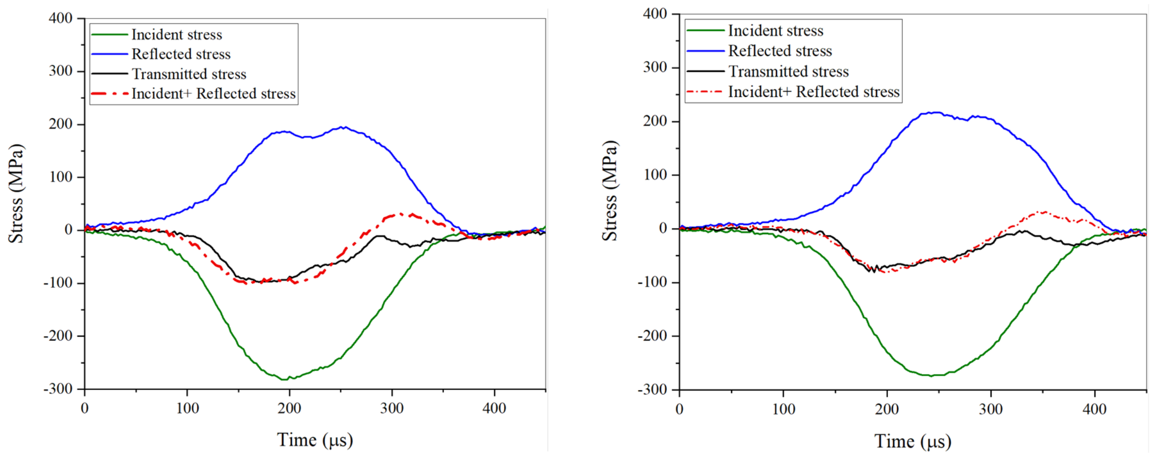

(a) Plain concrete (b) C60F40

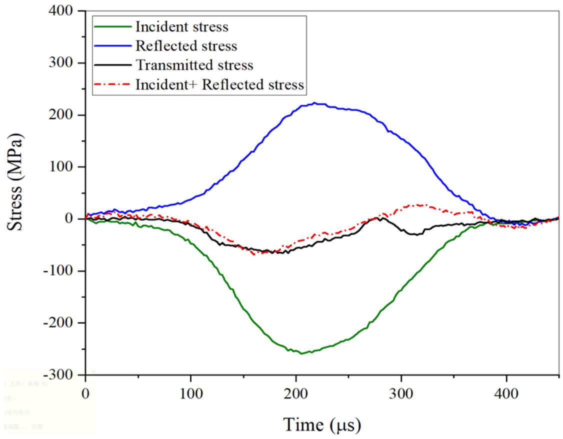

(c) C40F60

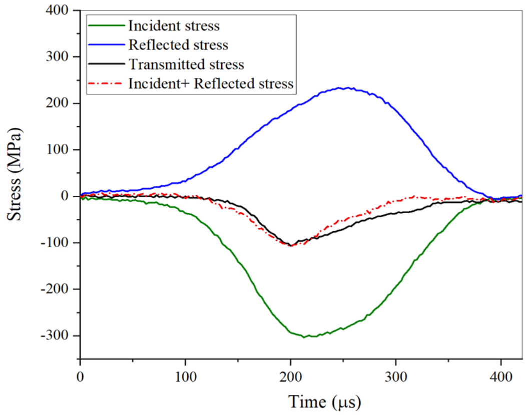

(d) C60F38N2

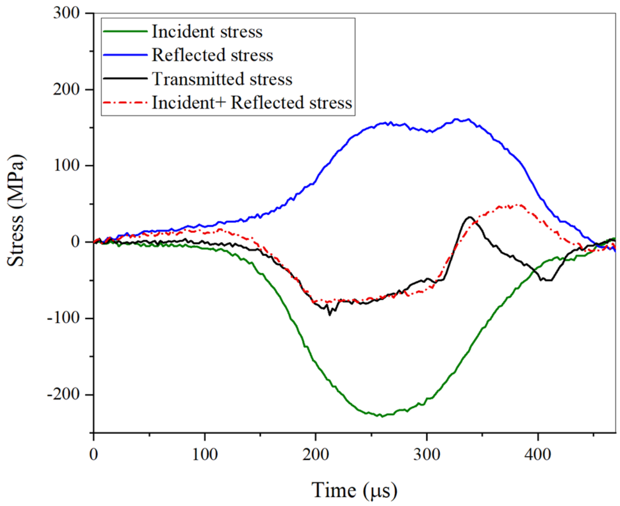

(e) C40F58N2

Fig. 6 (a)-(e). The strain rate and stress can be determined by the reflected signal and transmitted signal, respectively. In the previous studies [21-24], the strain rate of concrete-like material was determined corresponding to the time when the maximum compressive stress was reached as shown in Fig. 7, which was also used in this study.

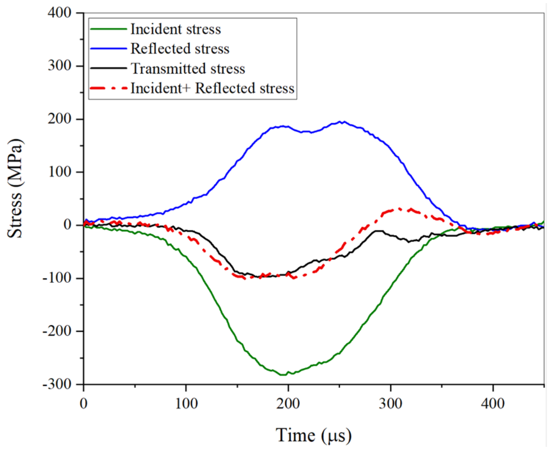

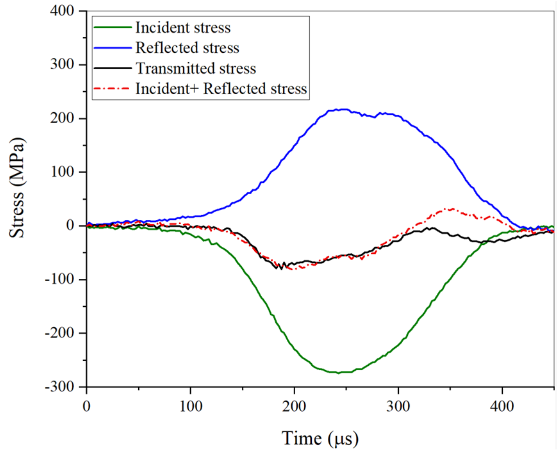

(f) Plain concrete (g) C60F40

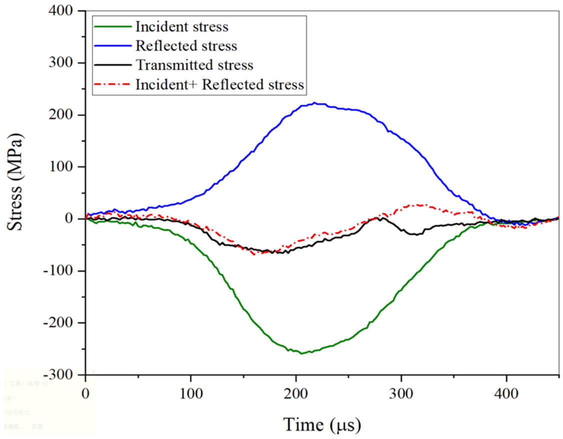

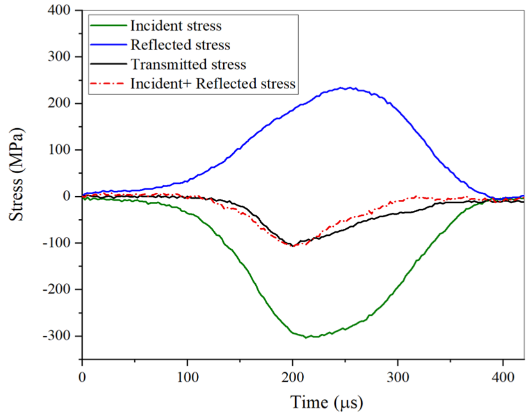

(h) C40F60 (i) C60F38N2

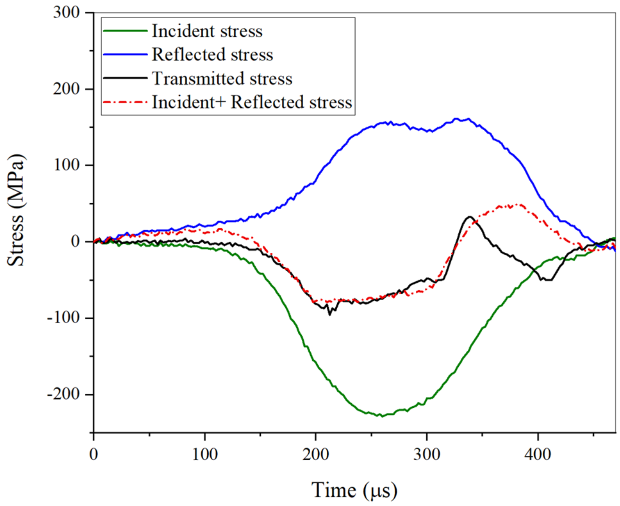

(j) C40F58N2

Fig. 6. Illustration of stress equilibrium of (a) plain concrete; (b) C60F40; (c) C40F60; (d) C60F38N2; (e) C40F58N2.

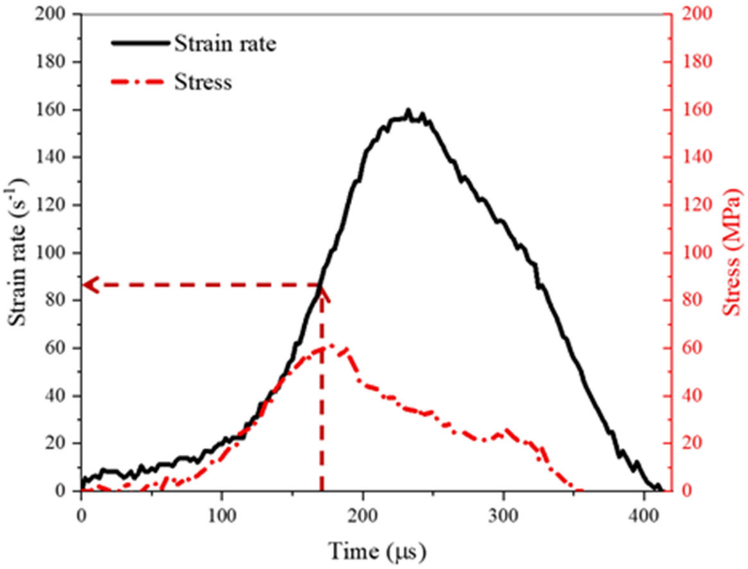

Fig. 7. Strain rate determination.

3.3. Failure process and failure mode

The failure process of all specimens under various strain rates was recorded and compared in Fig. 8 (a)-(e). 0 μs represents the moment when the specimen was initially stressed. The cracks initiated from the edges and extended to the mid region of the specimen. As observed, cracks appeared earlier with the increase of FA content. For instance, the specimen with 40% FA showed six minor cracks and the specimen with 60% FA showed ten minor cracks whereas only three minor cracks were observed on the specimen of plain concrete at 75 μs. As compared with the specimen of HVFA concrete without NS, C60F40, the replacement of 2% FA by NS delayed the occurrence of initial cracks, i.e. the specimen C60F38N2 showed only four minor cracks at 75 μs. This is because the dense microstructure of matrix was obtained by the filling effect of NS particles and the formation of calcium–silicate–hydrates (C–S–H) gel after replacing FA with NS, which significantly enhanced the compressive strength of HVFA concrete.

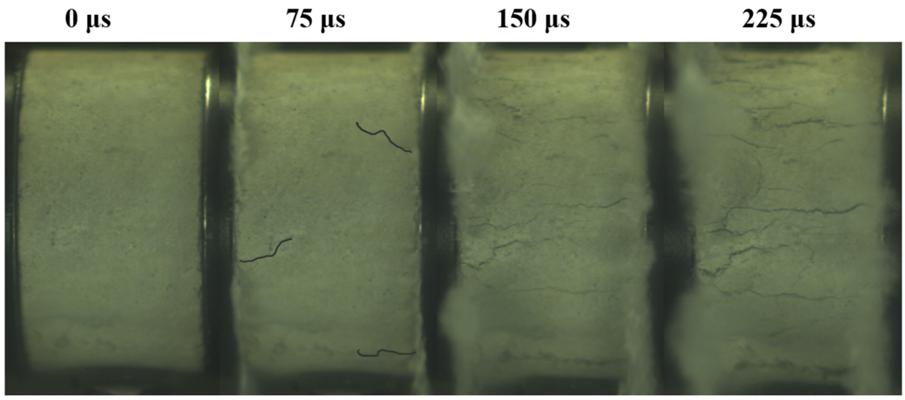

(a) Plain concrete

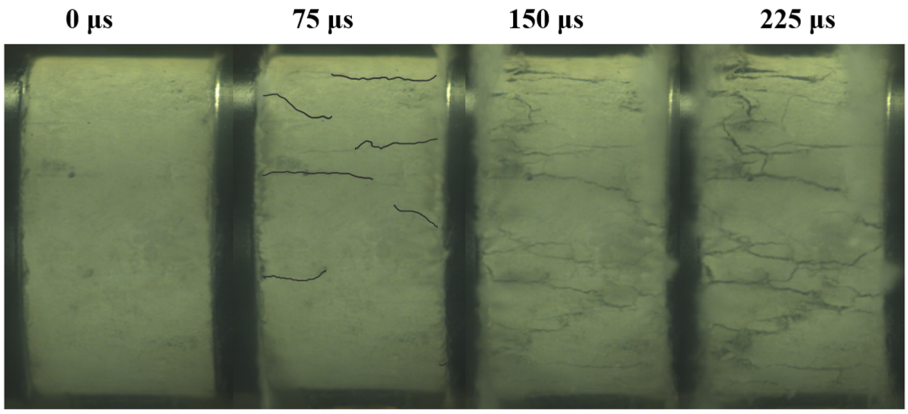

(b) C60F40

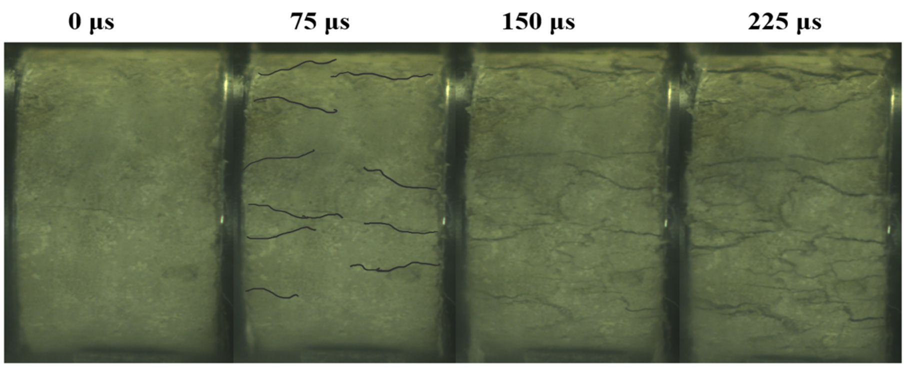

(c) C40F60

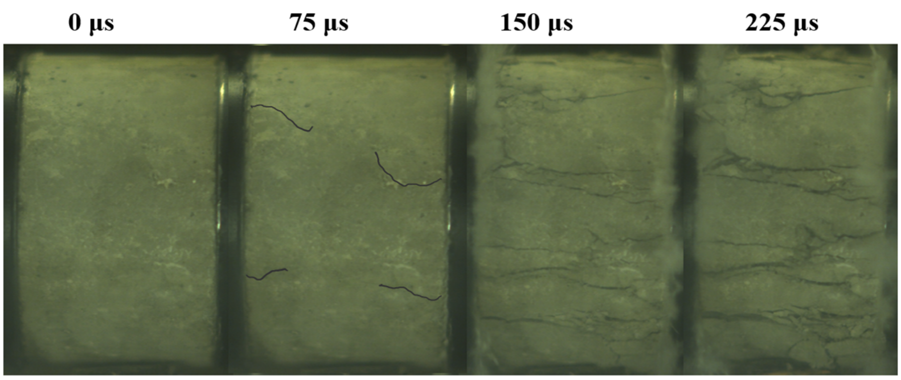

(d) C40F58N2

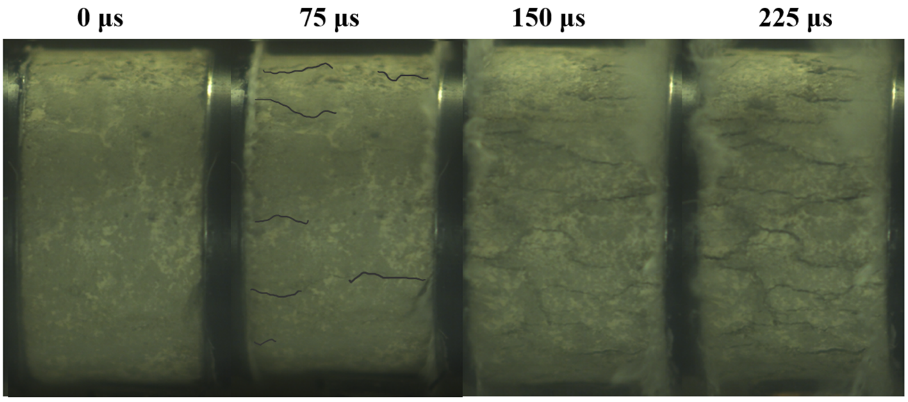

(e) C60F38N2

Fig. 8. Failure process of plain and HVFA concrete at the strain rate around 120 s^{-1}.
Note: the specimen size is 100 mm by 50 mm

The failure modes of plain and HVFA concrete with different FA contents and NS at different strain rates are compared in Fig. 9. It is observed that the damage level became more severe with the rising strain rate for each mix by experiencing partial crush, core remaining, crushing into pieces and pulverizing into fragments, respectively. The size of generated fragments depends on the imposed strain rate, which is consistent with the experimental results from the previous studies with respect to the strain rate effect on failure patterns of concrete-like materials [15, 22, 25, 26]. Various failure patterns of plain and HVFA concretes are due to different failure mechanisms at different strain rates. Fig. 10 shows three failure mechanisms of the specimen corresponding to different strain rates, i.e. matrix cracking, cracks cutting through aggregate, and fracture of aggregate. Under quasi-static and low strain rate, the cracks developed within the matrix, as shown in Fig. 10(a). The specimen then broken into large pieces without damaging the coarse aggregates. With the rising strain rate, the generated cracks propagated along shorter paths which resulted in cutting through coarse aggregates, as shown in Fig. 10 (b). When the strain rate further increased, a great portion of cracks developed by cleaving coarse aggregates and matrix into small pieces as shown in Fig. 10 (c).

At the similar strain rate, the damage level of the specimen became more severe with the increase of FA content. For instance, at the strain rate around 40 s^{-1}, the specimen HVFA concrete with 40% FA demonstrated better integrity than the HVFA concrete with 60% FA. Meanwhile, the specimen containing 2% NS showed better performance than the specimen without NS. For instance, the specimen of HVFA concrete with 40% FA shattered into several pieces while the failure mode of HVFA concrete with 38% FA and 2% NS is partially crushed under the strain rate around 50 s^{-1}. The dense microstructure resulted in fewer cracks by adding NS in the matrix.

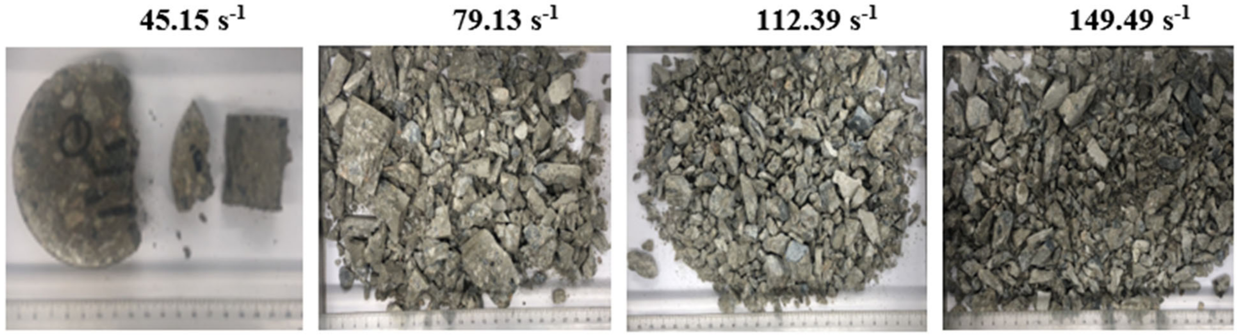

(a) Plain concrete

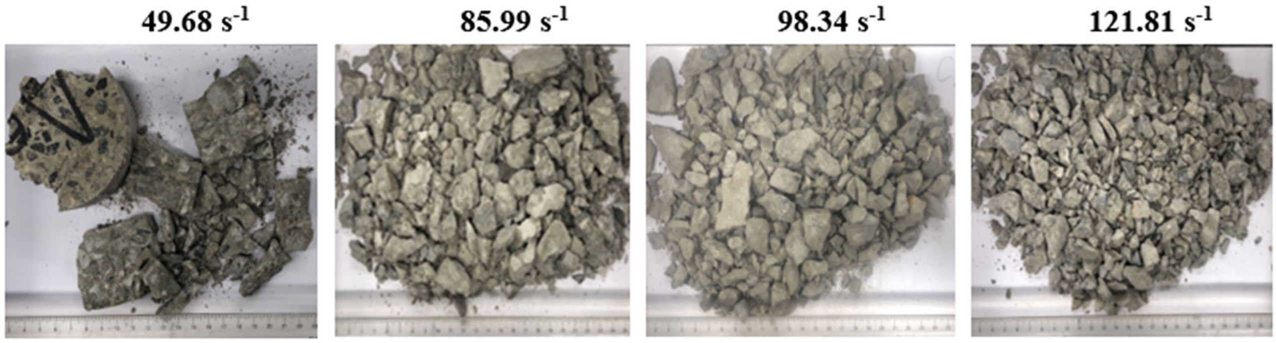

(b) C60F40

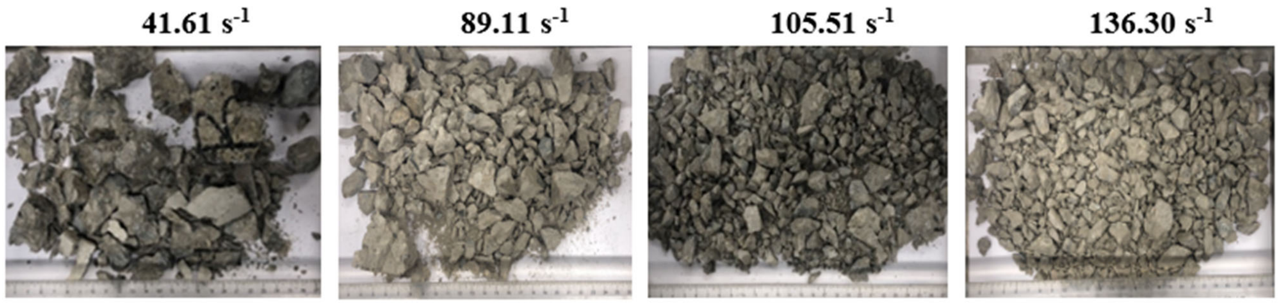

(c) C40F60

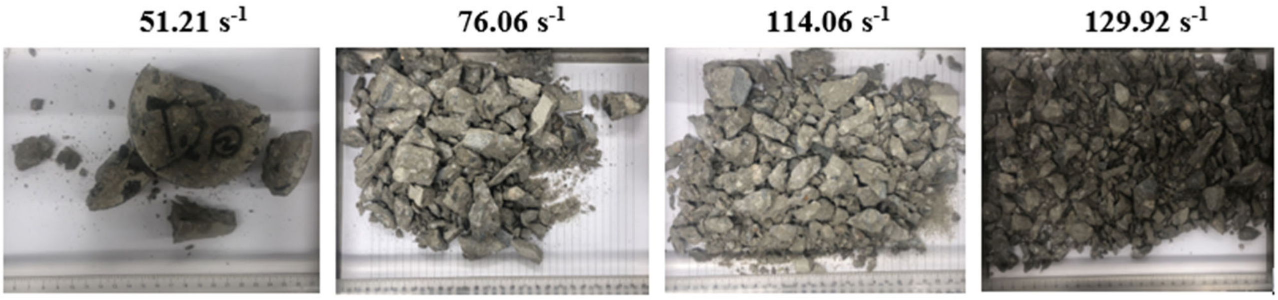

(d) C60F38N2

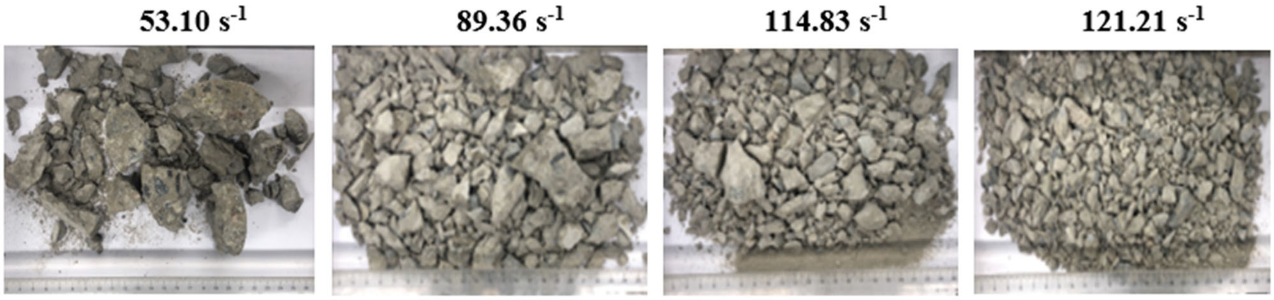

(e) C40F58N2

Fig. 9. Comparison of failure patterns of plain and HVFA concrete at various strain rates.

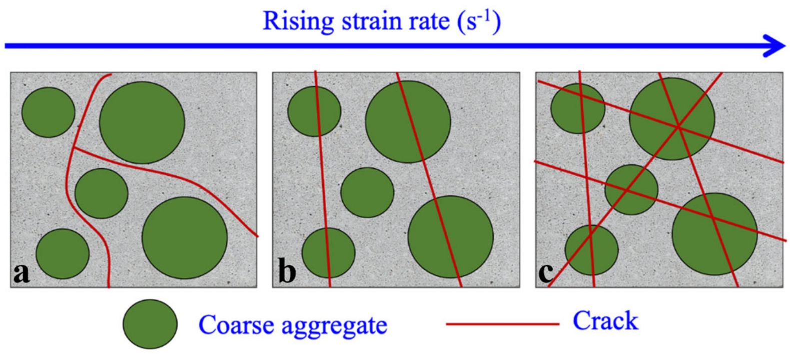

Fig. 10. Schematic diagram of failure modes with the rising strain rate. (a) cracks through the matrix; (b) cracks through coarse aggregates; (c) fracture of coarse aggregates.

3.4. Stress-strain relationships

Fig. 11 (a)-(e) show the stress-strain curves of HVFA concretes under dynamic compressive loads. As expected, dynamic compressive strength of all mixes increased with the rising strain rate, which was similar to the previous studies about strain rate effect on the dynamic compressive strength of concrete-like materials [22]. For instance, the compressive strength of HVFA concrete containing 40% FA content increased from 59.70 MPa at the strain rate of 49.68 s^{-1} to 95.72 MPa at the strain rate of 121.81 s^{-1}. The increase of strain rate leading to the higher compressive strength can be explained by the failure mechanism discussed in section 3.3. The dynamic compressive strength and energy absorption capacities of specimen can be enhanced by cracking through harder ingredients under higher strain rate loading.

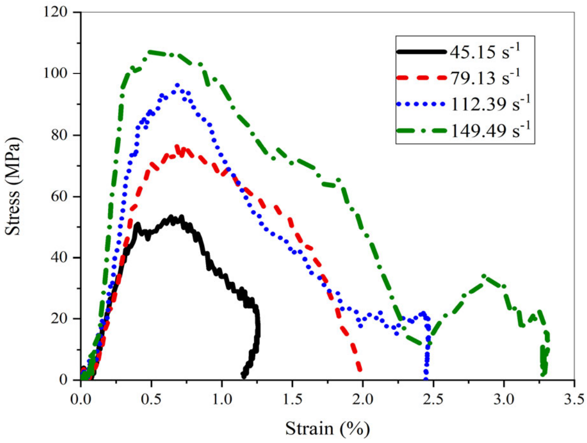

(a) PC

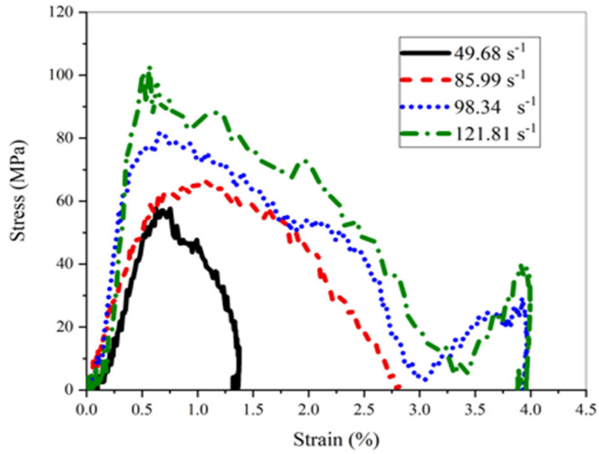

(b) C60F40

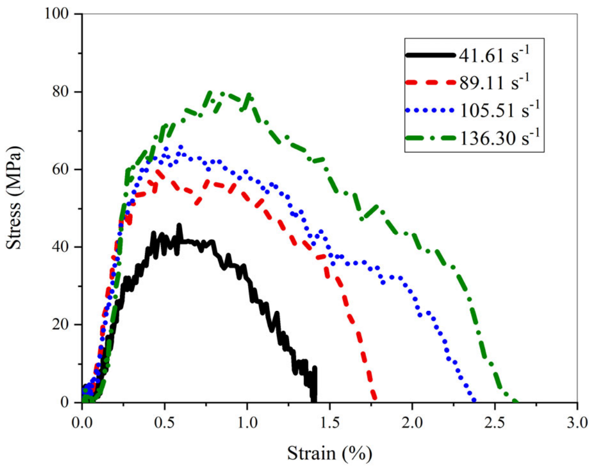

(c) C40F60

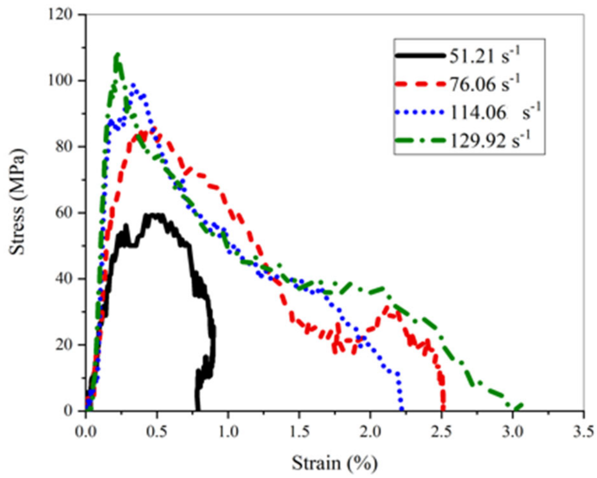

(d) C60F38N2

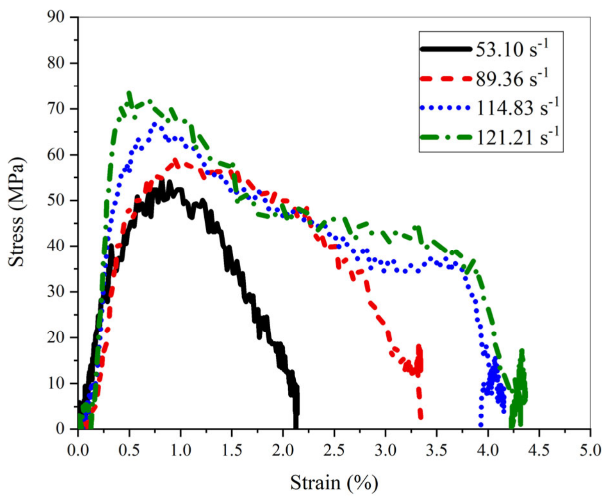

(e) C40F58N2

Fig. 11. Dynamic compressive stress–strain curves.

3.5. Comparison of strain rate effects on dynamic properties

Dynamic increase factor (DIF) of compressive strength can be obtained by normalizing dynamic compressive strength against quasi-static compressive strength. The peak stress of the stress-strain curve was defined as the dynamic compressive strength based on Eq. (1). However, the enhancement in the dynamic compressive strength was not only determined by the strain-rate effect of material but also the contribution from the end friction and the lateral inertia confinement [27]. In this study, the influence of the end friction effect was diminished by applying the grease between the pressure bars and the specimen. The contribution of lateral inertia confinement to the DIF for compressive strength was removed according to an empirical formula suggested in the previous study [28]. The results of all tests are summarized in Table 4 -Table 8.

Fig. 12 shows the relation between DIF of compressive strength and strain rates for plain and HVFA concretes. It is found that the DIF of all mixes was sensitive to the strain rate. For instance, the DIF of the HVFA concrete containing 40% FA was 1.86 at the strain rate of 49.68 s^{-1} and increased to 2.65 at the strain rate of 124.18 s^{-1}. This is attributed to different failure mechanisms at various strain rates elaborated in section 3.3. The DIF for compressive strength of OPC concrete can be predicted by the Euro-International Committee for Concrete (CEB) recommendation[29], which can be expressed as:

$$DIF_{fc} = \sigma_d/\sigma_s = (\dot{\varepsilon}_r/\dot{\varepsilon}_s)^{1.026\alpha_s} \; (\dot{\varepsilon}_r \le 30 \; s^{-1}) \quad (4)$$

$$DIF_{fc} = \sigma_d/\sigma_s = \gamma(\dot{\varepsilon}_r/\dot{\varepsilon}_s)^{1/3}\ (\dot{\varepsilon}_r\ > 30\ s^{-1}) \quad (5)$$

where $\dot{\varepsilon}_r$ is the strain rate (s^{-1}); $\dot{\varepsilon}_s$ = 30 × 10 $^{-6}$ s^{-1}; $\alpha_s = (5+9f_{sc}/10)^{-1}$; log γ = 6.156 α_s-2; f_{sc} is the quasi-static compressive strength. The DIFs for the compressive strength of plain and HVFA concretes are compared with the predication by the CEB recommendation for normal concrete [29] as shown in Fig. 12. The experimental results of plain and HVFA concretes fit well with the predictions by the CEB recommendation [29].

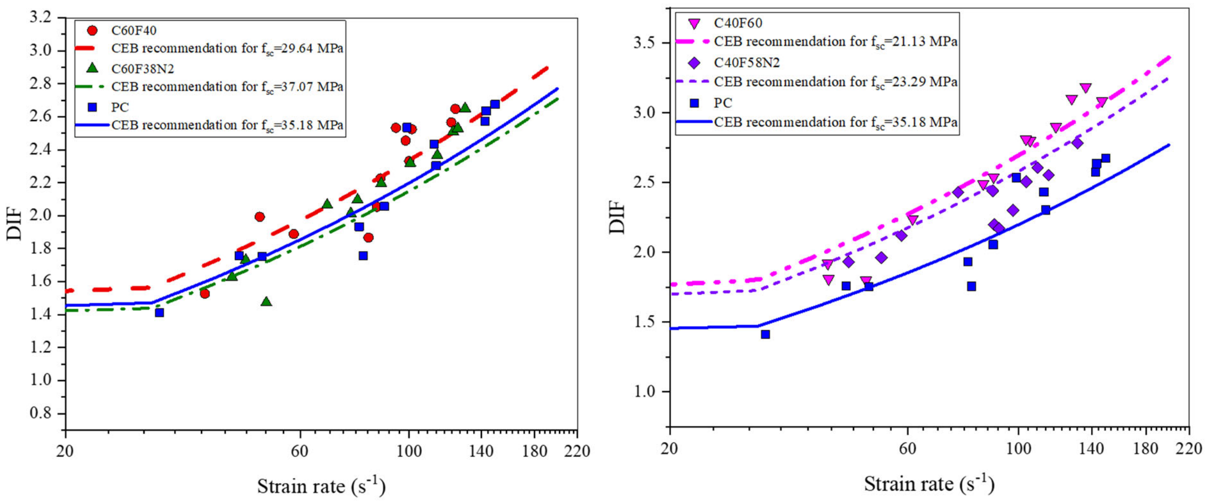

Fig. 12. Comparison of DIF for the compressive strength. (L) Plain concrete, C60F40 and C60F38N2; (R) Plain concrete, C40F60 and C40F58N2.

Fig. 12 compares the DIF for the compressive strength of HVFA concrete specimens with and without NS content. As shown, the DIF of HVFA concrete increased with the rising FA content and it was more sensitive to strain rate than that of plain concrete. The DIF of the specimens of HVFA concrete containing 2% NS was lower in general as compared to that of HVFA without NS. This is due to the micro-crack inertial mechanisms [30]. The matrix of HVFA concrete was a type of heterogeneous material consisting of cement and FA. More inherent micro-cracks and tiny voids were presented in the HVFA specimens due to the unreacted spherical shape of FA and the increased FA content. When subjected to higher strain rate loading, more cracks were developed from micro-cracks and tiny voids. As a result, the process of generating and spreading more cracks in the matrix would cause more energy dissipation, which resulted in higher compressive strength of the specimen. Shaikh et al. [9] conducted the microstructural analysis of the matrix of HVFA concrete containing NS by using the scanning electron microscopy (SEM) technique. It was reported that the adverse effect of pores or voids resulted from unreacted FA can be mitigated by the formation of secondary calcium silicate hydrate gels through the faster pozzolanic reaction of NS with calcium hydroxide. The specimen of NS modified HVFA concrete demonstrated dense microstructure without the observable pores and voids [31]. Therefore, the specimen with less micro-cracks increased the compressive strength but resulted in lower DIF of compressive strength under dynamic loading, which was consistent with the CEB recommendation. Furthermore, the test results of HVFA concrete containing NS conducted by Mussa et al. [15] were also compared as shown in Fig. 13. The DIF of HVFA concrete with NS in this study showed similar trend with the previous study. The HVFA concrete containing NS with higher quasi-static compressive strength of 58.72 MPa [15] than HVFA concrete in this study displayed a much lower DIF under the strain rate ranging from 30.5 s^{-1} to 85.5 s^{-1}. As shown in Fig. 13, the curve-fitting equations between DIF of compressive strength and strain rate ($\dot{\varepsilon}$) for plain and HVFA concretes within their corresponding strain rate ranges are listed below.

For plain concrete:

$$DIF = 0.796\ln(\dot{\varepsilon}) - 1.389 \quad \text{for } 31.10\ \text{s}^{-1} < \dot{\varepsilon} < 149.49\ \text{s}^{-1}\ (R^2 = 0.865) \qquad (6)$$

For C60F40:

$$DIF = 0.923\ln(\dot{\varepsilon}) - 1.862 \quad \text{for } 38.42\ \text{s}^{-1} < \dot{\varepsilon} < 124.18\ \text{s}^{-1}\ (R^2 = 0.802) \qquad (7)$$

For C40F60:

$$DIF = 1.092\ln(\dot{\varepsilon}) - 2.287 \text{ for } 41.48 \text{ s}^{-1} < \dot{\varepsilon} < 146.96 \text{ s}^{-1} \ (R^2 = 0.968) \quad (8)$$

For C60F38N2:

$$DIF = 0.918\ln(\dot{\varepsilon}) - 1.906 \text{ for } 43.62 \text{ s}^{-1} < \dot{\varepsilon} < 129.92 \text{ s}^{-1} \ (R^2 = 0.936) \quad (9)$$

For C40F58N2:

$$DIF = 0.717\ln(\dot{\varepsilon}) - 0.844 \text{ for } 45.60 \text{ s}^{-1} < \dot{\varepsilon} < 121.21 \text{ s}^{-1} \ (R^2 = 0.785) \quad (10)$$

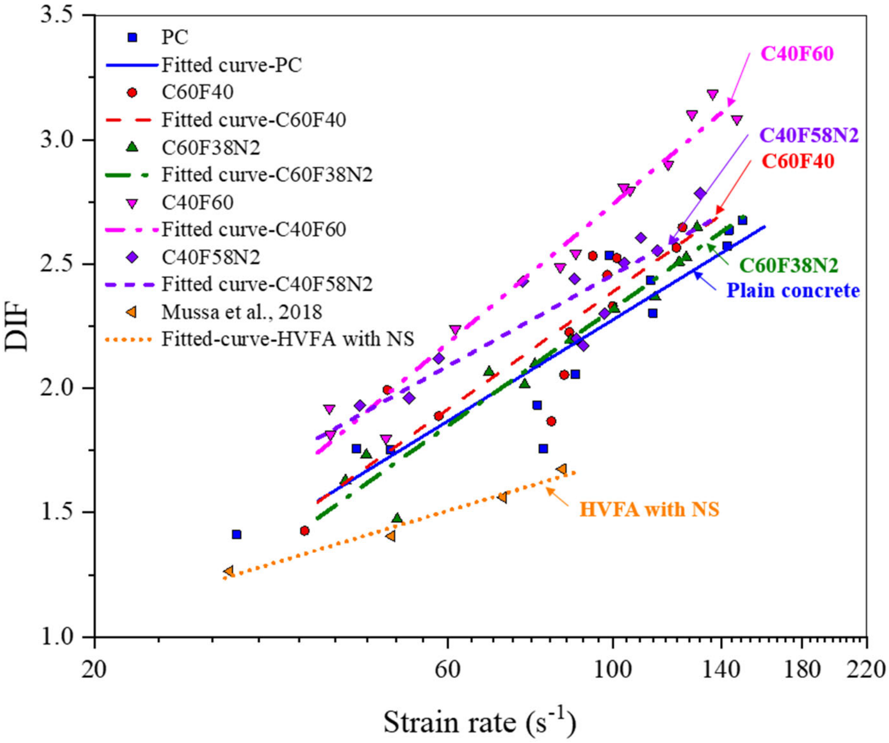

Fig. 13. Comparison of DIF for compressive strength from this study and the previous study [15].

Fig. 14 presents the relations between modulus of elasticity (E) and strain rate ($\dot{\varepsilon}$) for plain and HVFA concrete. It is observed that the modulus of elasticity for all mixes increased with the rising strain rate. For instance, the E value of the specimen of HVFA concrete containing 40% FA was 14.25 GPa at the strain rate of 49.68 s^{-1} and 27.89 GPa at the strain rate of 121.81 s^{-1}. The dynamic E value of HVFA concrete decreased with the increase of FA content subjected to the similar strain rate ranging from 30 to 140 s^{-1}. For instance, the modulus of elasticity of HVFA containing 60% FA was 15.33 GPa at the strain rate of 89.11 s^{-1}, while the modulus of elasticity of HVFA containing 40% FA was 18.42 GPa at the strain rate of 87.36 s^{-1}.

Additionally, the addition of NS improved the modulus of elasticity of HVFA concrete. For instance, under the strain rate of 40 s^{-1}, the E value of HVFA concretes containing 40% and 60% FA was 14.25 GPa and 12.21 GPa, respectively, while the 2% NS addition enhanced the E value of HVFA concretes with 38% and 58% FA content to 20.14 GPa and 15.36 GPa, respectively. It is worth noting that the E value of HVFA concrete C60F38N2 was higher than that of plain concrete, which indicates C60F38N2 can be an alternative to normal concrete. The curve-fitting equations between E and strain rate ($\dot{\varepsilon}$) for plain and HVFA concretes within their considered strain rate ranges are given as,

For plain concrete:

$$E = 11.452\ln(\dot{\varepsilon}) - 21.939 \quad \text{for } 31.10\ \text{s}^{-1} < \dot{\varepsilon} < 149.49\ \text{s}^{-1}\ (R^2 = 0.861) \tag{11}$$

For C60F40:

$$E = 8.564\ln(\dot{\varepsilon}) - 16.876 \quad \text{for } 38.42\ \text{s}^{-1} < \dot{\varepsilon} < 124.18\ \text{s}^{-1}\ (R^2 = 0.667) \tag{12}$$

For C40F60:

$$E = 6.791\ln(\dot{\varepsilon}) - 14.423 \quad \text{for } 41.48\ \text{s}^{-1} < \dot{\varepsilon} < 146.96\ \text{s}^{-1}\ (R^2 = 0.689) \tag{13}$$

For C60F38N2:

$$E = 12.607\ln(\dot{\varepsilon}) - 24.124 \quad \text{for } 43.62\ \text{s}^{-1} < \dot{\varepsilon} < 129.92\ \text{s}^{-1}\ (R^2 = 0.702) \tag{14}$$

For C40F58N2:

$$E = 7.289\ln(\dot{\varepsilon}) - 14.704 \quad \text{for } 45.60\ \text{s}^{-1} < \dot{\varepsilon} < 121.21\ \text{s}^{-1}\ (R^2 = 0.610) \tag{15}$$

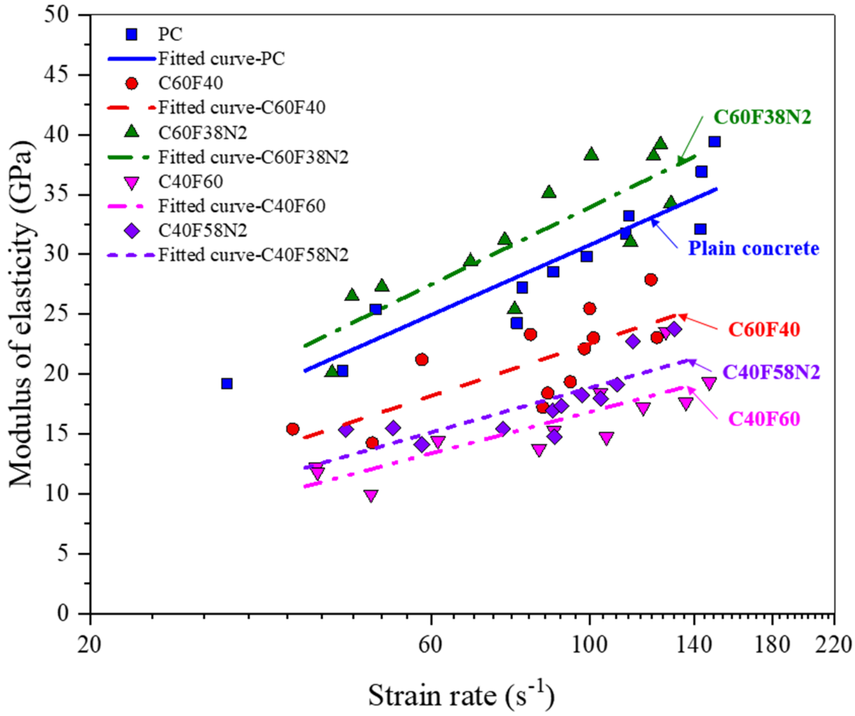

Fig. 14. Modulus of elasticity at different strain rates.

3.6. Energy absorption capability

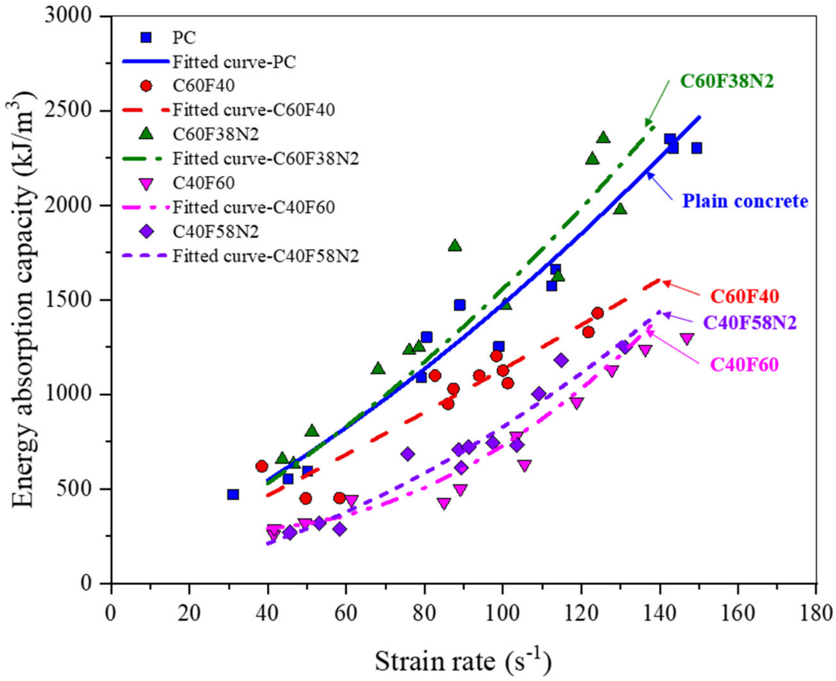

Fig. 15. Energy absorption at different strain-rates

Energy absorption capacities of concrete-like material are determined by ductility and strength [25]. The strain energy density was calculated to evaluate the energy absorption capability of plain and HVFA concrete. Therefore, the energy absorption capacities (*W*) can be calculated by the equation as given below,

$$W = \int_0^T \sigma(t) d\varepsilon(t) \quad (16)$$

where *σ(t)* is the time-dependent stress, and *ε(t)* is the time-dependent strain.

Fig. 15 presents the energy absorption capacities of plain and HVFA concretes with respect to strain rates. As observed, the energy absorption capacities increased with the rising strain rate for all mixes. It is found that the energy absorption capacities of HVFA concretes were lower than that of plain concrete and decreased with the increase of FA contents. The HVFA concrete containing 2% NS absorbed more energy than the corresponding HVFA concrete without NS due to the higher compressive strength. It is noted that the specimen C60F38N2 has the highest energy absorption capacity among all mixes at the same strain rate. The relationship between energy absorption capacities (W) and strain rate ($\dot{\varepsilon}$) within their corresponding strain rate ranges can be expressed as,

For plain concrete:

$$W = 0.038\dot{\varepsilon}^2 + 10.111\dot{\varepsilon} + 80.556 \quad (31.10\ s^{-1} < \dot{\varepsilon} < 149.49\ s^{-1})\ (R^2 = 0.969) \quad (17)$$

For C60F40:

$$W = 0.007\dot{\varepsilon}^2 + 10.105\dot{\varepsilon} + 51.527 \quad (38.42\ s^{-1} < \dot{\varepsilon} < 124.18\ s^{-1})\ (R^2 = 0.876) \quad (18)$$

For C40F60:

$$W = 0.096\dot{\varepsilon}^2 - 6.192\dot{\varepsilon} + 384.68 \quad (41.48\ s^{-1} < \dot{\varepsilon} < 146.96\ s^{-1})\ (R^2 = 0.942) \quad (19)$$

For C60F38N2:

$$W = 0.052\dot{\varepsilon}^2 + 9.775\dot{\varepsilon} + 55.567 \quad (43.62\ s^{-1} < \dot{\varepsilon} < 129.92\ s^{-1})\ (R^2 = 0.941) \quad (20)$$

For C40F58N2:

$$W = 0.049\dot{\varepsilon}^2 + 3.387\dot{\varepsilon} - 1.652 \quad (45.60\ s^{-1} < \dot{\varepsilon} < 121.21\ s^{-1})\ (R^2 = 0.927) \quad (21)$$

Table 4. Results of dynamic compressive tests for plain concrete (PC).

Specimen No.	Strain rate (s^{-1})	Dynamic compressive strength (MPa)	DIF_E	DIF_T	Young's modulus (GPa)	W (kJ/m^3)
PC-1	45.15	66.87	1.90	1.76	20.26	554.81
PC-2	31.10	53.18	1.51	1.41	19.21	472.12
PC-3	50.16	66.87	1.90	1.75	25.42	595.32
PC-4	79.13	74.95	2.13	1.93	24.26	1190.21
PC-5	80.56	68.17	1.94	1.76	27.22	1303.45
PC-6	88.96	80.14	2.28	2.06	28.54	1472.71
PC-7	98.98	99.34	2.82	2.53	29.84	1252.15
PC-8	113.41	90.92	2.58	2.30	33.23	1662.16
PC-9	112.39	96.02	2.73	2.43	31.73	1574.55
PC-10	143.46	105.67	3.00	2.64	36.92	2380.90
PC-11	142.70	103.10	2.93	2.57	32.12	2430.84
PC-12	149.49	107.55	3.06	2.68	39.42	2380.44

Note: DIF_E is the experimental results of DIF for compressive strength; DIF_T is the true DIF for compressive strength after removing lateral inertial confinement; W is the energy absorption capacity.

Table 5. Results of dynamic compressive tests for HVFA concrete with 40% FA (C60F40).

Specimen No.	Strain rate (s^{-1})	Dynamic compressive strength (MPa)	DIF_E	DIF_T	Young's modulus (GPa)	W (kJ/m^3)
C60F40-1	49.68	59.700	2.01	1.86	14.25	450.64
C60F40-2	58.27	60.971	2.06	1.89	21.22	453.09
C60F40-3	38.42	45.529	1.54	1.43	15.42	620.61
C60F40-4	87.36	73.03	2.46	2.23	18.42	13.73
C60F40-5	82.63	61.11	2.06	1.87	23.33	1100.82
C60F40-6	85.99	67.33	2.27	2.05	17.22	950.86
C60F40-7	93.98	83.39	2.81	2.53	19.36	1100.25
C60F40-8	100.00	77.00	2.60	2.33	25.48	1126.27

C60F40-9	98.34	81.03	2.73	2.46	22.12	1203.97
C60F40-10	124.18	88.55	2.99	2.65	23.07	1430.25
C60F40-11	121.81	95.72	3.23	2.87	27.89	1330.36
C60F40-12	101.23	83.43	2.82	2.52	23.03	1060.08

Table 6. Results of dynamic compressive tests for HVFA concrete with 60% FA (C40F60).

Specimen No.	Strain rate $\dot{\varepsilon}$ (s^{-1})	Dynamic compressive strength (MPa)	DIF_E	DIF_T	Young's modulus (GPa)	W (kJ/m^3)
C40F60-1	41.48	43.76	2.07	1.92	12.21	260.42
C40F60-2	41.61	41.34	1.96	1.81	11.82	290.07
C40F60-3	49.46	41.18	1.95	1.80	9.982	320.11
C40F60-4	89.11	59.54	2.82	2.54	15.33	624.31
C40F60-5	84.95	58.11	2.75	2.49	13.76	512.98
C40F60-6	61.32	51.64	2.44	2.24	14.44	463.76
C40F60-7	105.51	66.07	3.13	2.80	14.74	630.02
C40F60-8	103.43	66.26	3.14	2.81	18.43	780.16
C40F60-9	118.79	68.98	3.26	2.90	17.22	960.39
C40F60-10	146.96	74.39	3.52	3.08	19.33	1400.22
C40F60-11	127.79	74.11	3.51	3.10	23.56	1332.21
C40F60-12	136.30	80.03	3.62	3.19	17.63	1502.1

Table 7. Results of dynamic compressive tests for HVFA concrete with 38% FA and 2% NS (C60F38N2).

Specimen No.	Strain rate $\dot{\varepsilon}$ (s^{-1})	Dynamic compressive strength (MPa)	DIF_E	DIF_T	Young's modulus (GPa)	W (kJ/m^3)
C60F38N2-1	46.52	69.32	1.87	1.73	26.51	632.65
C60F38N2-2	51.21	59.26	1.60	1.47	27.32	552.86
C60F38N2-3	43.62	65.22	1.76	1.63	20.14	657.31
C60F38N2-4	68.12	83.84	2.26	2.07	29.42	1016.1
C60F38N2-5	76.06	82.15	2.22	2.01	31.22	1064.47

C60F38N2-6	78.51	85.64	2.31	2.10	25.42	1249.22
C60F38N2-7	100.50	95.84	2.59	2.32	38.28	1577.98
C60F38N2-8	114.06	98.54	2.66	2.37	31.03	1622.86
C60F38N2-9	87.71	90.08	2.43	2.19	35.12	1282.18
C60F38N2-10	122.84	104.85	2.83	2.51	38.22	2242.53
C60F38N2-11	125.60	105.81	2.85	2.53	39.19	2352.34
C60F38N2-12	129.92	111.09	3.00	2.65	34.27	1974.56

Table 8. Results of dynamic compressive tests for HVFA concrete with 58% FA and 2% NS (C40F58N2).

Specimen No.	Strain rate $\dot{\varepsilon}$ (s^{-1})	Dynamic compressive strength (MPa)	DIF_E	DIF_T	Young's modulus (GPa)	W (kJ/m^3)
C40F58N2-1	45.60	48.68	2.09	1.93	15.36	270.21
C40F58N2-2	53.10	49.62	2.13	1.96	15.48	320.42
C40F58N2-3	58.24	53.81	2.31	2.12	14.12	289.33
C40F58N2-4	88.72	62.99	2.70	2.44	16.962	710.24
C40F58N2-5	75.66	62.28	2.67	2.43	15.433	685.87
C40F58N2-6	89.34	56.78	2.44	2.20	14.789	612.26
C40F58N2-7	91.27	56.13	2.41	2.17	17.33	723.54
C40F58N2-8	97.45	59.67	2.56	2.30	18.24	745.07
C40F58N2-9	103.56	65.18	2.80	2.51	17.98	733.11
C40F58N2-10	109.17	67.97	2.92	2.61	19.14	1003.18
C40F58N2-11	114.83	66.80	2.87	2.55	22.74	1180.02
C40F58N2-12	121.21	73.47	3.15	2.78	23.78	1250.59

4. Conclusion

This study investigates the effect of adding 2% (by wt.) nano silica (NS) content on the static and dynamic properties of HVFA concretes containing 40% and 60% fly ash (FA). Dynamic failure process, failure mode and stress-strain curves of all mixes are compared with the strain rate up to 149.49 s^{-1}. The testing results demonstrate the strain rate sensitivity on the compressive strength, modulus of elasticity and energy absorption capacity for HVFA concrete. Based on the results, the main conclusions are summarized as follows.

1. Quasi-static compressive strength of HVFA concrete decreases by 15% and 40% with replacement of 40% and 60% of cement by FA, respectively. The failure process and failure pattern of HVFA concrete are strain rate dependent. With the increase of FA content, the cracking appears earlier, and the damage level becomes more severe at the similar strain rate.
2. Dynamic compressive strength, modulus of elasticity and energy absorption capacities of HVFA concretes are sensitive to strain rate. The DIF for compressive strength is higher with the increase of FA content. The compressive DIF of C60F40 and C40F60 can reach up to 2.65 and 3.10 at the strain rate of 124.18 s^{-1} and 127.79 s^{-1}, respectively. The modulus of elasticity and energy absorption capacities of HVFA concretes in general become lower with the increase of FA content at the similar strain rare.
3. The addition of 2% NS as partial replacement of FA in HVFA concretes containing 40% and 60% FA increases the quasi-static compressive strength and the enhancement is more significant for the one with 40% FA content. The addition of 2% NS delays the time of crack initiation, reduces the damage level and improves the dynamic compressive strength, modulus of elasticity and energy absorption capacity. Adding NS leads to the lower DIF for compressive strength of HVFA concrete.
4. The true DIF is obtained by removing the lateral inertia confinement effect from the experimental data. The true DIFs for the compressive strength of all mixes show good agreement with the predication by CEB recommendation. Empirical formulae are also

proposed to predict the compressive strength, modulus of elasticity and energy absorption capacity for all mixes.

5. The NS modified HVFA C60F38N2 has higher compressive strength, modulus of elasticity and energy absorption capacity than the plain concrete (PC), indicating the NS modified HVFA concrete material C60F38N2 can replace the normal concrete as a sustainable construction material.

Acknowledgements

The financial support from the Australian Research Council Laureate Fellowship FL180100196 is acknowledged.

Reference

[1] Reddy AN, Reddy PN, Kavyateja BV, Reddy GGK. Influence of nanomaterial on high-volume fly ash concrete: a statistical approach. Innovative Infrastructure Solutions. 2020;5(3):1-9.

[2] Shaikh FUA. Mechanical and durability properties of fly ash geopolymer concrete containing recycled coarse aggregates. International Journal of Sustainable Built Environment. 2016;5(2):277-87.

[3] Amran YM, Alyousef R, Alabduljabbar H, El-Zeadani M. Clean production and properties of geopolymer concrete; A review. Journal of Cleaner Production. 2020;251:119679.

[4] Li Z, Chen W, Hao H, Khan MZN. Physical and mechanical properties of new lightweight ambient-cured EPS geopolymer composites. Journal of Materials in Civil Engineering. Accpted 2020.

[5] McCarthy M, Dhir R. Development of high volume fly ash cements for use in concrete construction. Fuel. 2005;84(11):1423-32.

[6] ASTM. Standard Test Methods for Sampling and Testing Fly Ash or Natural Pozzolans for Use as a Mineral Admixture in Portland-Cement Concrete. ASTM C311-00. 2000.

[7] Nilsen AU, Monteiro PJ, Gjørv OE. Estimation of the elastic moduli of lightweight aggregate. Cement and Concrete Research. 1995;25(2):276-80.

[8] Burke D. Development of concrete mixtures with high-volume fly ash cement replacement. 2012 International Concrete Sustainability Conference, National Ready Mixed Concrete Association2012.

[9] Shaikh FUA, Supit SWM, Sarker PK. A study on the effect of nano silica on compressive strength of high volume fly ash mortars and concretes. Materials & Design. 2014;60:433-42.

[10] Kawashima S, Hou P, Corr DJ, Shah SP. Modification of cement-based materials with nanoparticles. Cement and Concrete Composites. 2013;36:8-15.

[11] Shaikh FUA, Supit SW. Chloride induced corrosion durability of high volume fly ash concretes containing nano particles. Construction and building materials. 2015;99:208-25.

[12] Li G. Properties of high-volume fly ash concrete incorporating nano-SiO2. Cement and Concrete research. 2004;34(6):1043-9.

[13] Zhang M-H, Islam J. Use of nano-silica to reduce setting time and increase early strength of concretes with high volumes of fly ash or slag. Construction and Building Materials. 2012;29:573-80.

[14] Zhou S, Zhang Y, Zhou D, Wang W, Li D, Ke Z. Experimental Study on Mechanical Properties of Fly Ash Stabilized with Cement. Advances in Civil Engineering. 2020;2020.

[15] Mussa MH, Mutalib AA, Hamid R, Raman SN. Dynamic properties of high volume fly ash nanosilica (HVFANS) concrete subjected to combined effect of high strain rate and temperature. Latin American Journal of Solids and Structures. 2018;15(1).

[16] Mussa MH, Abdulhadi AM, Abbood IS, Mutalib AA, Yaseen ZM. Late Age Dynamic Strength of High-Volume Fly Ash Concrete with Nano-Silica and Polypropylene Fibres. Crystals. 2020;10(4):243.

[17] ASTM. Standard Test Method for Relative Density (Specific Gravity) and Absorption of Fine Aggregate. ASTM C128-15. 2015.

[18] ASTM. Standard Test Method for Compressive Strength of Cylindrical Concrete Specimens. ASTM C39-18. 2018.

[19] Lv T, Chen X, Chen G. Analysis on the waveform features of the split Hopkinson pressure bar tests of plain concrete specimen. International Journal of Impact Engineering. 2017;103:107-23.

[20] Lindholm U. Some experiments with the split hopkinson pressure bar*. Journal of the Mechanics and Physics of Solids. 1964;12(5):317-35.

[21] Pham TM, Chen W, Khan AM, Hao H, Elchalakani M, Tran TM. Dynamic compressive properties of lightweight rubberized concrete. Construction and Building Materials. 2020;238.

[22] Hao Y, Hao H. Dynamic compressive behaviour of spiral steel fibre reinforced concrete in split Hopkinson pressure bar tests. Construction and Building Materials. 2013;48:521-32.

[23] Yin Z, Chen W, Hao H, Chang J, Zhao G, Chen Z, Peng K. Dynamic compressive test of gas-containing coal using a modified split hopkinson pressure bar system. Rock Mech Rock Eng. 2020;53(2):815-29.

[24] Li Z, Chen W, Hao H, Khan MZN, Pham TM. Dynamic compressive properties of novel lightweight ambient-cured EPS geopolymer composite. Construction and Building Materials. 2021;273:122044.

[25] Wang C, Chen W, Hao H, Zhang S, Song R, Wang X. Experimental investigations of dynamic compressive properties of roller compacted concrete (RCC). Construction and Building Materials. 2018;168:671-82.

[26] Zhang M, Wu H, Li Q, Huang F. Further investigation on the dynamic compressive strength enhancement of concrete-like materials based on split Hopkinson pressure bar tests. Part I: Experiments. International Journal of Impact Engineering. 2009;36(12):1327-34.

[27] Hao Y, Hao H, Jiang G, Zhou Y. Experimental confirmation of some factors influencing dynamic concrete compressive strengths in high-speed impact tests. Cement and Concrete Research. 2013;52:63-70.

[28] Hao Y, Hao H. Numerical evaluation of the influence of aggregates on concrete compressive strength at high strain rate. International Journal of Protective Structures. 2011;2(2):177-206.

[29] béton Ce-id, Précontrainte FIdl. CEB-FIP model code 1990: Design code: Thomas Telford Publishing; 1993.

[30] Khan MZN, Hao Y, Hao H, Shaikh FUA. Experimental evaluation of quasi-static and dynamic compressive properties of ambient-cured high-strength plain and fiber reinforced geopolymer composites. Construction and Building Materials. 2018;166:482-99.

[31] Behfarnia K, Salemi N. The effects of nano-silica and nano-alumina on frost resistance of normal concrete. Construction and Building Materials. 2013;48:580-4.